

Robust Partial-to-Partial Point Cloud Registration in a Full Range

Liang Pan¹ · Zhongang Cai^{1,2,3} · Ziwei Liu¹✉

Received: date / Accepted: date

Abstract Point cloud registration for 3D objects is a challenging task due to sparse and noisy measurements, incomplete observations and large transformations. In this work, we propose **Graph Matching Consensus Network (GMCNet)**, which estimates pose-invariant correspondences for full-range Partial-to-Partial point cloud Registration (PPR) in the object-level registration scenario. To encode robust point descriptors, **1)** we first comprehensively investigate transformation-robustness and noise-resilience of various geometric features. **2)** Then, we employ a novel Transformation-robust Point Transformer (**TPT**) module to adaptively aggregate local features regarding the structural relations, which takes advantage from both handcrafted rotation-invariant (*RI*) features and noise-resilient spatial coordinates. **3)** Based on a synergy of hierarchical graph networks and graphical modeling, we propose the Hierarchical Graphical Modeling (**HGM**) architecture to encode robust descriptors consisting of i) a unary term learned from *RI* features; and ii) multiple smoothness terms encoded from neighboring point relations at different scales through our TPT modules. Moreover, we construct a challenging PPR dataset (**MVP-RG**) based on the recent MVP dataset that features high-quality scans. Extensive experiments show that GMCNet outperforms previous state-of-the-art methods for PPR. Notably, GMCNet encodes point descriptors for each point cloud individually without using cross-contextual information, or ground truth correspondences for training. Our code and datasets are available at <https://github.com/paul007pl/GMCNet>.

Keywords Object-Centric Point Cloud Registration · Robust Point Descriptors · Partial Object Scans · 3D Point Transformer

1 Introduction

Point cloud registration (PCR) is a fundamental task for a wide range of applications such as localization (Droeschel and Behnke 2018; Yang et al. 2018; Ding and Feng 2019), 3D reconstruction (Wan et al. 2018; Lu et al. 2019) and 6D object pose estimation (Wong et al. 2017; Tian et al. 2020), where a rigid transformation (*i.e.*, a 3D rotation and a 3D translation) is estimated to align a source point cloud to a target point cloud. Classic methods that leverage Iterative Closest Point algorithm require a good transformation initialization and usually prune to local minima. With the advent of deep learning, researchers are encouraged to creating learning models for solving PCR.

A series of learning-based PCR methods (Wang and Solomon 2019a,b; Li et al. 2019; Yew and Lee 2020; Fu et al. 2021) have been proposed. In the object-centric PCR scenario, Wang et. al. (Wang and Solomon 2019a,b) learn to encode point features for estimating a mapping between the source point cloud and the target from ModelNet40 dataset (Wu et al. 2015). Instead of directly taking 3D coordinates as inputs, recent PCR methods, RPMNet (Yew and Lee 2020), DeepGMR (Yuan et al. 2020) and IDAM (Li et al. 2019), provide better registration results with the help of rotation-invariant (*RI*) features. However, most of them (except DeepGMR) are only validated under restricted source-target transformations (*i.e.*, rotations in $[0, 45^\circ]$). According to our experiments, large transformations could undermine their training stability, and also largely increase registration error. Although DeepGMR could handle PCR

¹ S-Lab, Nanyang Technological University, Singapore

² Sensetime Research

³ Shanghai AI Lab.

Corresponding author: Ziwei Liu
ziwei.liu@ntu.edu.sg

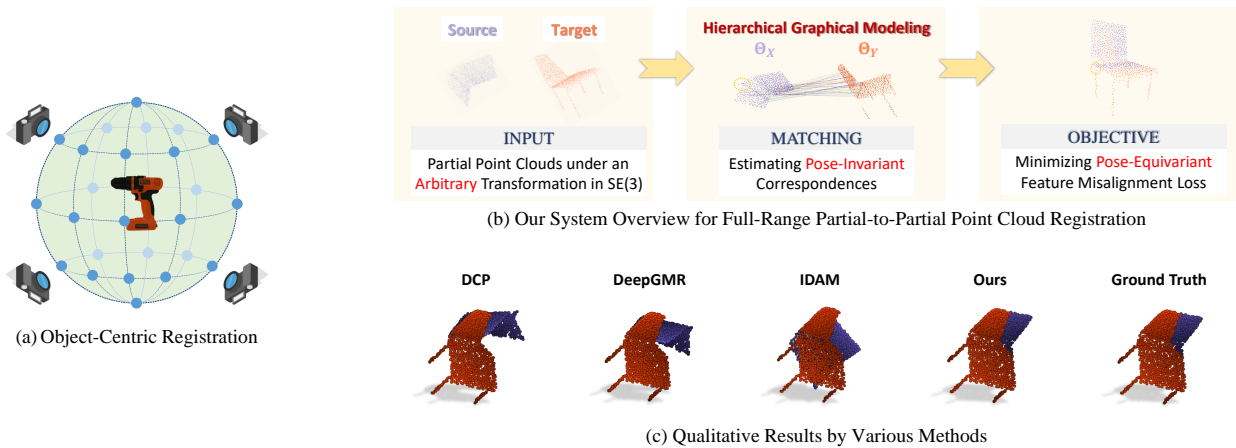


Fig. 1: (a) Object-Centric Registration Application. Object 6D-pose estimation is an example application that often requires to register partial point clouds under large transformations, which are observed from diverse viewpoints. **(b) System Overview.** Our GMCNet learns robust feature descriptors for full-range Partial-to-Partial point cloud Registration (PPR). **(c) Qualitative Comparison.** Qualitative results for full-range PPR on ModelNet40 (Wu et al. 2015) by various methods, including DCP (Wang and Solomon 2019a), DeepGMR (Yuan et al. 2020), IDAM (Li et al. 2019) and GMCNet.

with large transformations for complete point clouds, partial point clouds significantly degrade its registration performance. In practice, unconstrained viewpoints give rise to large transformations (*e.g.*, Fig. 1 (a) demonstrates arbitrary transformations in the $SE(3)$) along with noisy measurements and partial observations, which are the key challenges for PCR. In this work, we take one step further and focus on partial-to-partial point cloud registration (PPR) in the *full-range*¹, which are more relevant to real-world applications.

Encoding robust and discriminative point feature descriptors against large transformations and noisy measurements could be the major difficulty in estimating correct correspondences for global registration. Motivated by the success of using *RI* features for unconstrained arbitrary rotations in 3D object classification (Drost et al. 2010; Chen et al. 2019; Li et al. 2021) and 3D molecule property prediction (Fuchs et al. 2020; Satorras et al. 2021), we find *RI* features promising, given carefully designed network architectures, to outperform existing methods (Yew and Lee 2020; Yuan et al. 2020; Li et al. 2019) for full-range PPR. To better understand the advantages and limitations of conventional coordinate encoding and various handcrafted *RI* features (including *RRI*, *FPFH* and *PPF*), we start by analyzing their robustness against arbitrary transformations and random noises. On the one hand, we observe that *RI* features between different partial point clouds with arbitrary $SE(3)$ transformations could be no longer invariant, but they are still more transformation-robust than coordinate encoding. On the other hand, *RI* features are much more sensi-

tive to noise than coordinate features. Despite that *RI* features are inconsistent due to different noisy observations, *RI* features with jitters augmentations could facilitate *RI* classification (Chen et al. 2019; Li et al. 2021), and hence we speculate that they still describe *RI* 3D geometric properties. In addition, global and relative spatial coordinates of point clouds show superior noise-resilient properties, which results in stable structural relations. In view of this, we are motivated to match robust distribution-level features learned from structured *RI* features for global PPR.

Equipped with the findings from the preliminary study, we develop our approach to full-range PPR. We represent point cloud as a set of features with graph structures, and the correspondence estimation for PPR is reformulated as a maximum common subgraph prediction problem. Specifically, we propose a one-shot paradigm, Graph Matching Consensus Network (**GMCNet**), which estimates pose-invariant correspondences (Fig. 1 (b)) using *RI* features and multi-scale graph structures for full-range PPR. In order to encode large-scale distribution features, we enlarge the receptive fields by consecutively sub-sampling point clouds in a hierarchical architecture. To tackle the uncertainty introduced in the sub-sampling process, *e.g.* Farthest Point Sampling (FPS)² that leads to inconsistent encoded features, we employ a novel Transformation-robust Point Transformer (**TPT**) module, which adaptively aggregates neighboring features from sampled points with the help of both *RI* feature graphs and noise-resilient spatial relations. Following the idea of graphical modeling, we further propose the Hierarchical Graphical Modeling (**HGM**) architecture that encodes robust descriptors for each point consisting of: 1) a unary term learned from *RI* features; and 2) mul-

¹ In this paper, full-range transformation and global transformation are used interchangeably, both refer to arbitrary transformations in $SE(3)$.

² FPS usually initials the sampling with the first point.

multiple smoothness terms to encourage spatially-smooth correspondences with multi-scale geometric distribution-level features.

Moreover, following the recent MVP dataset (Pan et al. 2021), we construct a challenging object-centric PPR benchmark dataset (dubbed **MVP-RG**) consisting of 7,600 high-quality point cloud pairs. Compared with the standard object-centric benchmark dataset, ModelNet40 (Wu et al. 2015), partial point clouds in MVP-RG are generated by high-resolution virtual cameras from diverse viewpoints, which better imitates real observations than uniformly sampling used for ModelNet40. Experimental results on ModelNet40 and MVP-RG dataset show that GMCNet outperforms previous state-of-the-art (SoTA) methods. Qualitative results for full-range PPR on ModelNet40 by various methods are shown in Fig. 1 (c), where GMCNet achieve accurate registration in spite of noisy and partial observation. We highlight that GMCNet employs a one-shot paradigm for PPR, and it encodes robust descriptors for each point cloud individually without requiring cross-contextual information. In other words, the processing of each point clouds is self-sufficient and does not require information of the other point cloud in the source-target pair. Besides, no ground truth correspondences are needed during training.

The key contributions are summarized as:

- We comprehensively analyze transformation-robustness and noise-resilience of different geometric features, which paves the way to encode robust descriptors for global PPR.
- Employing graphical modeling in the context of deep learning, we propose a novel hierarchical graph network (dubbed GMCNet) by employing novel TPT modules, which encodes robust geometric feature descriptors.
- Extensive experimental results show that GMCNet achieves much better registration results than previous SoTA methods, especially for full-range PPR.
- A challenging object-centric PPR benchmark dataset (MVP-RG) is constructed, which consists of 7,600 paired high-quality partial point clouds generated by using virtual cameras from various viewpoints.

2 Related Work

2.1 Rotation-Invariant (*RI*) Features

Learning *RI* features has been extensively studied. By defining local reference frames (LRF), many descriptors (Chen and Bhanu 2007; Frome et al. 2004; Johnson and Hebert 1999; Salti et al. 2014; Tombari et al. 2010) accumulate measurements into histograms according to spatial coordinates, surface normals and curvatures. However, it is difficult to achieve rotation-invariance by defining unambiguous LRFs. Without relying on LRFs, researchers designed

handcrafted *RI* features, such as *PPF* (Drost et al. 2010), *PFH* (Rusu et al. 2008) and *FPFH* (Rusu et al. 2009). With the help of deep learning, robust *RI* descriptors can be encoded based on the handcrafted features for downstream tasks (Deng et al. 2018b,a; Zhao et al. 2019; Chen et al. 2019). For example, networks designed with *RRI* features show impressive performance for classification (Chen et al. 2019) and registration (Yuan et al. 2020; Sun et al. 2020). In addition, a few recent works (Choy et al. 2019; Gojcic et al. 2019; Bai et al. 2020) study on encoding geometric features with deep networks, while they mainly focus on learning 3D point descriptors from large-scale dense 3D point clouds.

2.2 Deep Point Cloud Registration (PCR)

Conventional PCR methods mainly use the ICP (Besl and McKay 1992) and its variants (Rusinkiewicz and Levoy 2001; Segal et al. 2009; Bouaziz et al. 2013; Pomerleau et al. 2015). However, these methods (Besl and McKay 1992; Rusinkiewicz and Levoy 2001; Segal et al. 2009; Bouaziz et al. 2013; Pomerleau et al. 2015) only can register point clouds under a small relative transformation, as they prune to local minima. To guarantee a global optima, complicated optimization approaches, such as branch-and-bound (Yang et al. 2013), convex relaxation (Maron et al. 2016), line process (Zhou et al. 2016) and semidefinite programming (Yang and Carlone 2019), are proposed.

In the object-centric scenario, many learning-based PCR methods are proposed recently. Comparing to non-learning methods, many learning PCR methods could achieve better object-centric registration. PointNetLK (Aoki et al. 2019) and PCRNet (Sarode et al. 2019b,a) iteratively regress the rotation and translation using global features encoded by PointNet (Qi et al. 2017). DCP (Wang and Solomon 2019a) and PRNet (Wang and Solomon 2019b) generate the estimated transformation by predicting soft assignments between two point sets with encoded features by DGCNN (Wang et al. 2019). Other follow-up works (Yew and Lee 2020; Li et al. 2019) iteratively resolve PPR with robust descriptors encoded by *RI* features. Nonetheless, most existing methods (Aoki et al. 2019; Sarode et al. 2019b,a; Wang and Solomon 2019a,b; Yew and Lee 2020; Li et al. 2019, 2020; Jiang et al. 2021; Bauer et al. 2021; Xu et al. 2021) focus on local PCR (*i.e.*, rotations in $[0, 45^\circ]$), while overlooking global PCR. Additionally, they prefer to learn point descriptors without using hierarchies for sparse object-centric PPR. DeepGMR (Yuan et al. 2020) addresses full-range PCR for complete point clouds by using pose-invariant GMM latent correspondences. However, different partial point clouds mostly do not have the same GMM variables, which makes it inapplicable for PPR.

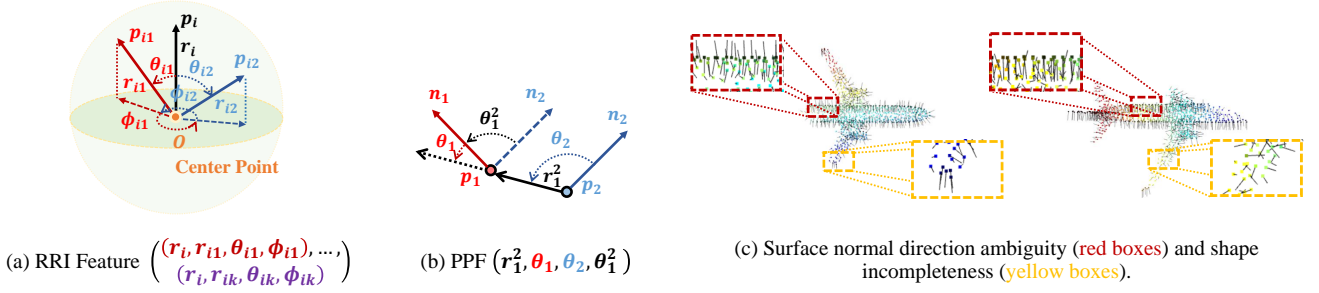


Fig. 2: Handcrafted Rotation-Invariant Features. (a) *RRI* (Chen et al. 2019) r_i denotes the distance between p_i and O (e.g. $\|p_i\|_2$). r_{ik} denotes the distance between the k^{th} nearest neighbor of p_i and O . θ and ϕ are angles between p_i and its neighboring points. (b) *PPF* (Drost et al. 2010) r_1^2 is the distance $\|p_1 - p_2\|_2$. θ_1 and θ_2 are $\angle(\overline{p_1 p_2}, \overline{n_1})$ and $\angle(\overline{p_1 p_2}, \overline{n_2})$, respectively. θ_1^2 is $\angle(\overline{n_1}, \overline{n_2})$, the angle between $\overline{n_1}$ and $\overline{n_2}$. (c) Inconsistent surface normal estimation usually consists of 1. surface normal direction ambiguity ((red boxes)); 2. shape incompleteness (yellow boxes); and 3. inconsistent measurements that often caused by different 3D scans or noisy measurements.

3 Problem Analysis

Following previous object-centric registration methods, in this work, we focus on small-scale object-centric point cloud registration. In this section, we first formulate the Partial-to-Partial point cloud Registration (PPR), and then introduce various pose-invariant point features. Finally, we analyze the transformation-robustness and noise-resilience of different handcrafted features.

3.1 Partial-to-Partial Point Cloud Registration (PPR)

Given a source point cloud $\mathcal{X} = \{x_1, \dots, x_N\} \subset \mathbb{R}^3$ and a target point cloud $\mathcal{Y} = \{y_1, \dots, y_M\} \subset \mathbb{R}^3$, PCR targets at aligning \mathcal{X} to \mathcal{Y} , i.e. mapping each x_i to $y_{m(x_i)}$, by finding a rigid transformation $\mathbf{T}_{\mathcal{X}\mathcal{Y}} = [\mathbf{R}_{\mathcal{X}\mathcal{Y}}, \mathbf{t}_{\mathcal{X}\mathcal{Y}}]$ comprising a rotation $\mathbf{R}_{\mathcal{X}\mathcal{Y}} \in \text{SO}(3)$ and a translation $\mathbf{t}_{\mathcal{X}\mathcal{Y}} \in \mathbb{R}^3$. If \mathcal{X} and \mathcal{Y} are two different *partial* point clouds with overlapped areas, it becomes the more challenging PPR problem, as more outliers are introduced by their different partial observations. Previous methods (Wang and Solomon 2019b; Yew and Lee 2020) address the registration problem by alternating between two steps: 1) predicting a mapping m between \mathcal{X} and \mathcal{Y} ; 2) estimating current optimal rotation $\mathbf{R}_{\mathcal{X}\mathcal{Y}}$ and translation $\mathbf{t}_{\mathcal{X}\mathcal{Y}}$ with the mapped inliers $\mathcal{X}_{in} \subset \mathcal{X}$ and $\mathcal{Y}_{in} \subset \mathcal{Y}$. Given a predicted mapping m , the optimal $\mathbf{R}_{\mathcal{X}\mathcal{Y}} = \mathbf{V}\mathbf{U}^\top$ and $\mathbf{t}_{\mathcal{X}\mathcal{Y}} = -\mathbf{R}_{\mathcal{X}\mathcal{Y}} \cdot \bar{x} + \bar{y}$ can be optimized by using a singular value decomposition (SVD), $\mathbf{U}\mathbf{S}\mathbf{V}^\top = \mathcal{F}_{\text{SVD}}(\mathbf{H})$, where the cross-covariance matrix $\mathbf{H} = \sum_{x_i \in \mathcal{X}_{in}} (x_i - \bar{x}) \cdot (y_{m(x_i)} - \bar{y})^\top$, $\bar{x} = \frac{1}{|\mathcal{X}_{in}|} \sum_{x_i \in \mathcal{X}_{in}} x_i$ and $\bar{y} = \frac{1}{|\mathcal{Y}_{in}|} \sum_{y_j \in \mathcal{Y}_{in}} y_j$. To estimate the mapping m , learning-based methods (Wang and Solomon 2019a,b; Yew and Lee 2020; Li et al. 2019) match their encoded deep features:

$$m(x_i, \mathcal{Y}) = \mathcal{F}_{\text{map}}[\text{softmax}(\Theta_{\mathcal{Y}} \cdot \Theta_{x_i}^\top)], \quad (1)$$

where $\mathcal{F}_{\text{map}}[\cdot]$ denotes a learnable mapping function, $\Theta_{\mathcal{X}} \in \mathbb{R}^{N \times C}$ and $\Theta_{\mathcal{Y}} \in \mathbb{R}^{M \times C}$ are embedded feature descriptors for each point in \mathcal{X} and \mathcal{Y} , respectively.

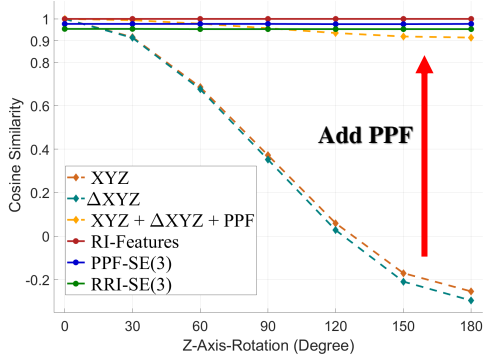
3.2 Pose-Invariant Features

To estimate accurate correspondences between \mathcal{X} and \mathcal{Y} , it is important to encode $\Theta_{\mathcal{X}}$ and $\Theta_{\mathcal{Y}}$ that are robust and even invariant to arbitrary transformations $\mathbf{T} = [\mathbf{R}, \mathbf{t}] \in \text{SE}(3)$. Previous networks (Drost et al. 2010; Zhang et al. 2019; Chen et al. 2019) on 3D perception tasks can obtain $\text{SO}(3)$ -invariance with the help of handcrafted *RI* features, such as *RRI* (Chen et al. 2019) and *PPF* (Drost et al. 2010).

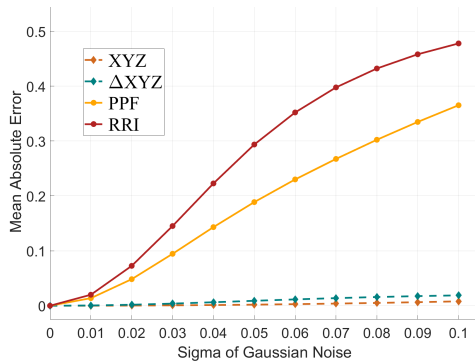
Global RI feature. As a global *RI* feature, *RRI* achieves pose-invariance³ in accordance to a origin-centered unit sphere that usually uses the shape center of a point cloud as the coordinate center “ O ” (Fig. 2 (a)). Because complete point clouds under arbitrary transformations have the same shape center, its translation-invariance can be guaranteed by translating complete point clouds to the same origin-centered unit sphere coordinate. However, different partial point clouds mostly have inconsistent shape centers caused by different missing parts, which challenges the pose-invariance of *RRI*.

Local RI feature. Different from *RRI*, *PPF* features measure local pose-invariant point pairs relations, such as relative distances and surface normal deviations (Fig. 2 (b)), which is invariant under arbitrary $\mathbf{R} \in \text{SO}(3)$ and $\mathbf{t} \in \mathbb{R}^3$. Similar to *PPF*, *FPFH* (Rusu et al. 2009) encodes pose-invariant geometric properties by using average curvature of the multi-dimensional histogram around a center point locally. Both *PPF* and *FPFH* rely on the presence of consistent surface normal estimations. Although we can estimate surface normals on-the-fly using local neighboring points, the surface normal direction ambiguities (red boxes)

³ Pose-invariance consists of rotation- and translation-invariance.



(a) Pose-Invariance Analysis



(b) Noise-Sensitivity Analysis

Fig. 3: Handcrafted Feature Analysis on Pose and Noise. (a) Handcrafted rotation-invariant features can highly increase rotation-robustness, but a SE(3) transformation (*i.e.*, rotations and translations) can slightly influence their invariance. (b) Absolute position “XYZ” and relative position “ Δ XYZ” are more robust against noisy measurements than rotation-invariant features.

and 3D shape incompleteness (yellow boxes) make the normal estimation inconsistent, especially in the object-centric scenario (Fig. 2 (c)). Moreover, noisy measurements make pose-invariant correspondences estimation more challenging.

3.3 Transformation-Robustness and Noise-Resilience

To investigate robustness of various features against (a) arbitrary transformations and (b) random noise, we conduct a preliminary study (Fig. 3) on the ModelNet40 test set with 2,468 complete point clouds (2,048 points).

Rotation-Robustness. For rotation-robustness, a rotation axis (*e.g.*, Z-axis) is fixed, and then we gradually increase the rotation magnitude from 0° to 180° . Handcrafted *RI* features (*e.g.*, *RRI*, *PPF* and *FPFH*) are invariant against arbitrary rotations (see red line), but the absolute position “XYZ” and the relative position “ Δ XYZ” are highly influenced by the increment in the rotation magnitude. Furthermore, concatenating the *RI* features, such as *PPF*, with

“XYZ” and “ Δ XYZ” can highly increase the rotation-robustness⁴ (yellow dash line). However, if adding an arbitrary translation, the similarity scores “PPF-SE(3)” and “RRI-SE(3)” will be influenced (*i.e.* <1) due to ambiguous surface normal directions and mismatched shape centers, respectively. *FPFH* is similar with *PPF*, and hence we omitted it in Fig. 3 (a). Nonetheless, handcrafted *RI* features can still describe *RI* geometric properties (such as local curvatures and smoothness) for the corresponding observation, because “PPF-SE(3)” and “RRI-SE(3)” are invariant to arbitrary rotations, and showing two horizontal lines (blue line and green line) in Fig. 3 (a).

Noise-Resilience. As for noise-resilience test (Fig. 3 (b)), we add a random Gaussian noise $N(0, \sigma^2)$ to each point of point clouds, and gradually increases the σ from 0 to 0.1. The mean absolute error shows that handcrafted *RI* features are much more influenced by noise than “XYZ” and “ Δ XYZ” by comparing each feature channel discrepancy with the increasing noise. Hence, “XYZ” and “ Δ XYZ” could be more noise-resilient, which represents stable 3D geometrical structures for the point clouds.

Analysis. According to our experiments, inconsistent measurements caused by center shifting, normal direction ambiguity or random noise, could influence the transformation-robustness of *RI* features. Although being robust against noisy measurements, global or relative coordinate features could be highly influenced by large transformations. On the other side, coordinate-based features could serve as stable feature structure for organizing *RI* features. Moreover, we notice that many networks (Zhang et al. 2019; Chen et al. 2019; Li et al. 2021; Zhang et al. 2022) utilize *RI* features along with random Gaussian noise for *RI* classification, and it reveals that noise would not largely influence the shape semantics for grouped points. Consequently, aggregating distribution-level features with *RI* features and noise-resilient structural relations is promising to increase descriptor robustness in terms of arbitrary poses and random noise. However, previous methods (Yuan et al. 2020; Deng et al. 2018b; Yew and Lee 2020; Li et al. 2019) face difficulties in solving full-range PPR of noisy and incomplete point clouds. We argue that it is critical to construct network architecture that leverage the synergy between handcrafted *RI* and coordinate features for transformation-robust and noise-resilient descriptors for global PPR.

4 Our Approach

We represent point cloud as a list of neighborhood graphs $\{\mathcal{N}\}$, and each $\mathcal{N} = (\mathcal{V}, \mathcal{E}, \mathbf{X})$ consists of a node set \mathcal{V} for spatial coordinates, an edge set \mathcal{E} for neighboring con-

⁴ Similar observations are reported in PPFNet (*e.g.*, Table 6) (Deng et al. 2018b).

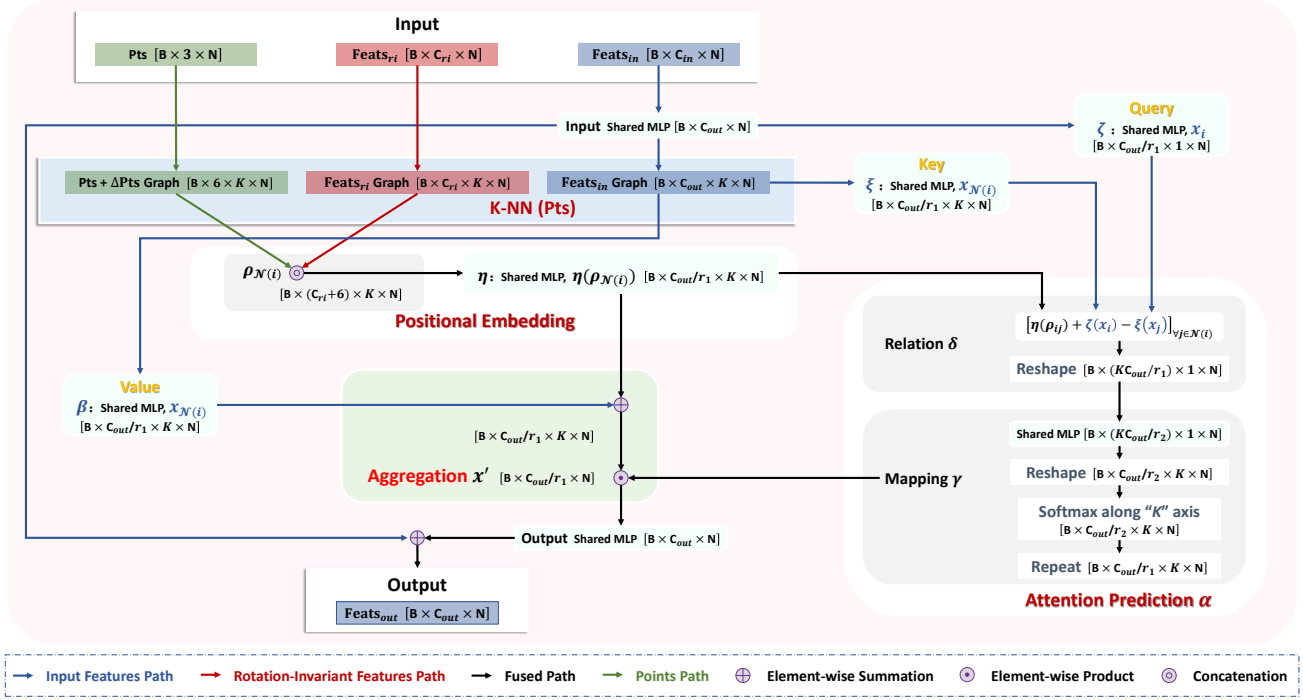


Fig. 4: Transformation-robust Point Transformer (TPT) module. TPT adaptively integrates point features by using various neighborhood graphs. The feature tensor size is illustrated in detail, where “B”, “C”, “K” and “N” are the number of batches, feature channels, neighboring points and total points, respectively. r_1 and r_2 are two hyper-parameters (e.g., 4 and 8) for adjusting the attention weights that can be shared across a group of channels.

nections and a node feature set \mathbf{X} for encoded descriptors. Consequently, the two partial point clouds \mathcal{X} and \mathcal{Y} are represented as two lists of neighborhood graphs $\{\mathcal{N}_s = (\mathcal{V}_s, \mathcal{E}_s, \mathbf{X})\}$ and $\{\mathcal{N}_t = (\mathcal{V}_t, \mathcal{E}_t, \mathbf{Y})\}$, and estimating pose-invariant correspondences between \mathcal{X} and \mathcal{Y} can be reformulated as a maximal common graph estimation problem between $\{\mathcal{N}_s\}$ and $\{\mathcal{N}_t\}$ by using noise-resilient graph structures and transformation-robust node features.

4.1 Transformation-Robust Point Transformer

To encode robust point feature descriptors, we propose a novel Transformation-robust Point Transformer (TPT) module, which adaptively aggregates local features by considering both point feature similarities and their spatial positions for each neighborhood graph \mathcal{N} . Notably, the neighborhood relationships \mathcal{E} in point clouds are also pose-invariant. In contrast to previous point cloud transformer operations (Guo et al. 2021; Zhao et al. 2021) that are designed for 3D perception tasks, TPT emphasizes the pose-robustness for the aggregated point features by using hand-crafted *RI* features in the positional encoding. The attention-based aggregation layer of TPT (Fig. 4) can be formulated

as follows:

$$\mathbf{x}'_i = \sum_{j \in \mathcal{N}(i)} (\beta(\mathbf{x}_j) + \eta(\rho_{ij})) \odot \alpha(\mathbf{x}_{\mathcal{N}(i)}, \eta(\rho_{\mathcal{N}(i)}))_j, \quad (2)$$

where β and η are shared Multi-Layer-Perceptrons (MLPs), $\mathcal{N}(i)$ is the K-Nearest Neighboring (K-NN) point graph constructed in the spatial coordinates for the center point x_i , $\beta(\mathbf{x}_j)$ is the transformed features, $\eta(\rho_{ij})$ is the positional embedding, $\alpha(\mathbf{x}_{\mathcal{N}(i)}, \eta(\rho_{\mathcal{N}(i)}))_j$ denotes the attention weight $w_{ij} = \gamma(\delta(\mathbf{x}_{\mathcal{N}(i)}, \eta(\rho_{\mathcal{N}(i)})))_j$, and \odot is element-wise product. In view that vector attention operators (Zhao et al. 2020) often achieve better performance than scalar attention operators (Vaswani et al. 2017), we compute a vector attention that adapts to different feature channels, which consists of a relation operator δ and a mapping function γ :

$$\delta(\mathbf{x}_{\mathcal{N}(i)}, \eta(\rho_{\mathcal{N}(i)})) = [[\zeta(\mathbf{x}_i) - \xi(\mathbf{x}_j) + \eta(\rho_{ij})]_{\forall j \in \mathcal{N}(i)}], \quad (3)$$

where ζ and ξ are shared MLPs, and δ combines all feature vectors by concatenation, which is equivalent to the “Reshape” operation in Fig. 4. Afterwards, γ further transforms the set of vectors, and then maps to the right dimensionality. Particularly, we carefully design the positional encoding for describing the positional relations between pairwise

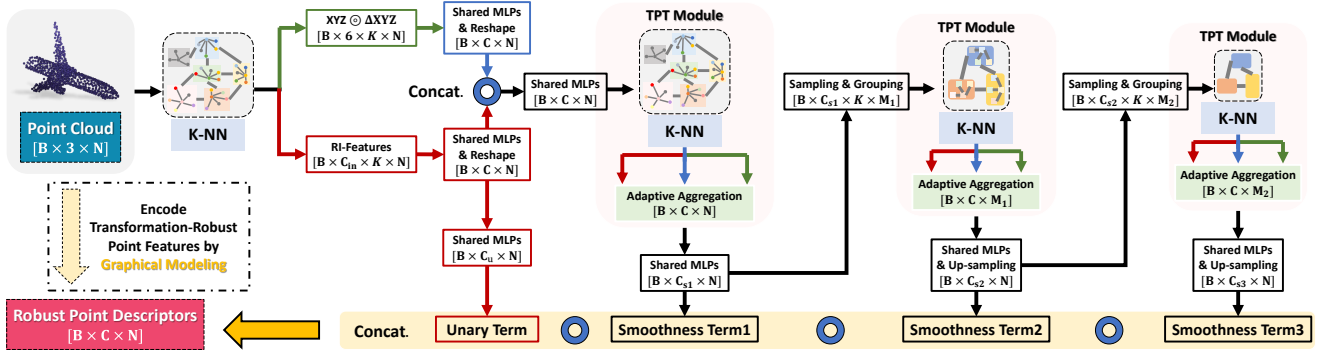


Fig. 5: Hierarchical Graphical Modeling for Encoding Transformation-Robust Feature Descriptors. Following the graphical modeling structure, each point descriptor consists of 1) a “Unary Term” learned by the rotation-invariant feature graphs; 2) and multiple “Smoothness Terms” encoded from neighboring geometric features at different scales.

connected points by concatenating the absolute positions, relative positions and handcrafted *RI* features (e.g. *RRI* and *PPF*). Although adding absolute and relative positions may influence the pose-invariance, it further increases PPR performance against noise.

4.2 Hierarchical Graphical Modeling

A probabilistic graphical model utilizes a graph-based representation to express conditional dependency among random variables, which can encode a distribution over a multi-dimensional space with the graph structure (Koller and Friedman 2009). Given that a point cloud can be represented as a set of neighborhood graphs $\{\mathcal{N}\} = \{(\mathcal{V}, \mathcal{E}, \mathbf{X})\}$, we propose a Hierarchical Graphical Modeling (HGM) architecture to encode multi-scale distribution features for constructing robust point feature descriptors for the source and the target individually. As shown in Fig. 5, the constructed descriptors for each point consist of 1) a unary term focusing on each node learned by handcrafted *RI* features graphs; 2) multiple smoothness terms focusing on 3D geometric distributions encoded from multi-scale structural relations using the proposed TPT modules (similar with the *Sum-Product* (Koller and Friedman 2009)). Consequently, the encoded descriptors for a point point x_i can be formulated as:

$$\Theta_{x_i} = \left[\Omega(\mathbf{x}_{\mathcal{N}_1(i)}^{\text{RI}}), A^1(\mathbf{x}_{\mathcal{N}_1(i)}), A^2(\mathbf{x}_{\mathcal{N}_2(i)}), A^3(\mathbf{x}_{\mathcal{N}_3(i)}) \right], \quad (4)$$

where Θ_{x_i} concatenates the unary term $\Omega(\cdot)$ encoded by *RI* features $\mathbf{x}_{\mathcal{N}_1(i)}^{\text{RI}}$, and the smoothness terms $A^1(\cdot)$, $A^2(\cdot)$ and $A^3(\cdot)$. $\mathcal{N}_1(i)$, $\mathcal{N}_2(i)$ and $\mathcal{N}_3(i)$ are neighborhood graphs at different scales. Accordingly, the mapping function m estimation can be formulated as an assignment problem with

the following objective function:

$$E(m) = \sum_{x_i \in \mathcal{X}} \left(\lambda_u E_u(\Omega(\mathbf{x}_{\mathcal{N}_1(i)}^{\text{RI}}), \Omega(\mathbf{Y}_{\mathcal{N}_1(i)}^{\text{RI}})) \right. \\ \left. + \sum_n \lambda_{s_n} E_{s_n}(A^n(\mathbf{x}_{\mathcal{N}_n(i)}), A^n(\mathbf{Y}_{\mathcal{N}_n(i)})) \right), \quad (5)$$

where $E_u(\cdot)$ denotes the unary penalty term, $E_{s_n}(\cdot)$ denotes each smoothness penalty term, and $\lambda(\cdot)$ is the corresponding weights for each term.

Unlike previous methods (Deng et al. 2018b; Yew and Lee 2020) that only use the nearest neighbor as the paired points to encode handcrafted *RI* features, we consider each point as a centroid that is paired with more neighboring points for $\Omega(\cdot)$. We highlight that our unary term $\Omega(\cdot)$ rigorously preserves rotation-invariance, which can resolve full-range PCR without smoothness terms if the measurements are clean and consistent. The smoothness terms $A^n(\cdot)$ is transformation-robust with the help of *RI* features, which highly increases noise-resilience for optimizing the mapping function m .

4.3 Optimization

Mapping Function Optimization. We penalize the mismatching loss by encouraging correspondences with similar feature descriptors. For each potential mapping $m(x_i, y_j)$, we compute element-wise feature distances between corresponding terms from $\Theta_{\mathcal{X}}$ and $\Theta_{\mathcal{Y}}$:

$$E(m_{ij}) = \sum_{\mathcal{C}} \left(\lambda_u (\|\Omega(\mathbf{x}_{\mathcal{N}_1(i)}^{\text{RI}}) - \Omega(\mathbf{y}_{\mathcal{N}_1(j)}^{\text{RI}})\|_2 / \sqrt{|\mathcal{C}_u|}) \right. \\ \left. + \sum_n \lambda_{s_n} (\|A^n(\mathbf{x}_{\mathcal{N}_n(i)}) - A^n(\mathbf{y}_{\mathcal{N}_n(j)})\|_2 / \sqrt{|\mathcal{C}_{s_n}|}) \right), \quad (6)$$

where $|\mathcal{C}_u|$ and $|\mathcal{C}_{s_n}|$ are the feature size for each corresponding feature item, which adjusts their importance.

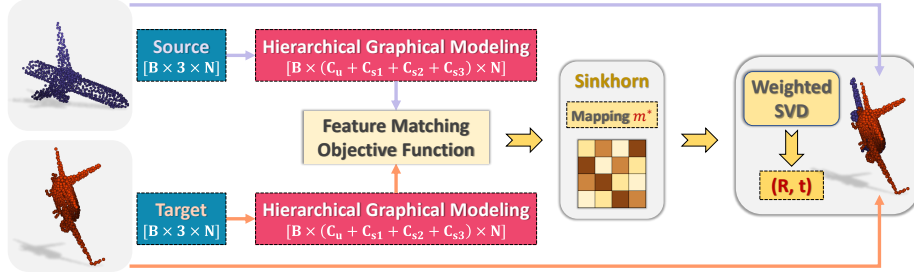


Fig. 6: Framework Overview. GMCNet estimates pose-invariant correspondences using the robust feature descriptors encoded by our HGM. Note that the two HGM share weights.

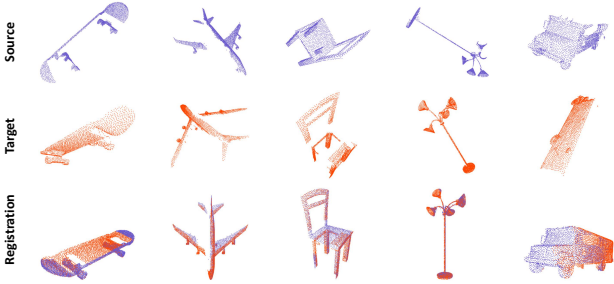


Fig. 7: Data examples in MVP-RG dataset. The source point clouds and the target are different partial scans under a relative transformation in SE(3) for the same object.

Hence, $m(x_i, y_j)$ is initialized as $\exp(-E(m_{ij}))$. Thereafter, we use Sinkhorn normalization layers for outlier rejection (Santa Cruz et al. 2017; Sarlin et al. 2020; Yew and Lee 2020). With the optimized matching matrix m^* , the cross-covariance matrix $\mathbf{H} = \sum_{i=1}^N c_i \cdot (x_i - \bar{x}) \cdot (y[m^*(x_i)] - \bar{y})^\top$, where $\bar{x} = \sum_{i=1}^N c_i \cdot x_i$, $\bar{y} = \sum_{i=1}^N c_i \cdot y[m^*(x_i)]$, $y[m^*(x_i)] = \frac{1}{\sum_j m^*(x_i, y_j)} \sum_j y_j \cdot m^*(x_i, y_j)$, and $c_i = \sum_j m^*(x_i, y_j)$, which denotes the confidence for point x_i is an inlier. In the end, $\mathbf{R}_{\mathcal{X}\mathcal{Y}}$ and $\mathbf{t}_{\mathcal{X}\mathcal{Y}}$ can be resolved by a SVD introduced in Sec. 3. Consequently, our GMCNet framework overview can be illustrated in Fig. 6.

Training Loss. GMCNet is trained end-to-end. Following (Yew and Lee 2020), the training loss consists of two parts, a registration loss \mathcal{L}_{RG} and an auxiliary loss \mathcal{L}_{IL} to encourage inliers. In addition, we further improves registration estimation by using a cycle loss function that is formulated as:

$$\mathcal{L} = \mathcal{L}_{\text{RG}} + \omega \mathcal{L}_{\text{IL}} = \mathcal{L}_{\text{reg}}^{\mathcal{X}\mathcal{Y}} + \mathcal{L}_{\text{reg}}^{\mathcal{Y}\mathcal{X}} + \omega(\mathcal{L}_{\text{inlier}}^{\mathcal{X}\mathcal{Y}} + \mathcal{L}_{\text{inlier}}^{\mathcal{Y}\mathcal{X}}), \quad (7)$$

where $\mathcal{L}_{\text{reg}}^{\mathcal{X}\mathcal{Y}} = \frac{1}{N} \sum_i^N |\mathbf{T}_{\text{pred}}^{\mathcal{X}\mathcal{Y}}(x_i) - \mathbf{T}_{\text{GT}}^{\mathcal{X}\mathcal{Y}}(x_i)|$, $\mathbf{T}_{\text{pred}}^{\mathcal{X}\mathcal{Y}}$ is our predicted transformation for $\mathcal{X} \rightarrow \mathcal{Y}$, $\mathcal{L}_{\text{inlier}}^{\mathcal{X}\mathcal{Y}} = \frac{1}{M} \sum_j^M (1 - \sum_i^N m^*(x_i, y_j)) + \frac{1}{N} \sum_i^N (1 - \sum_j^M m^*(x_i, y_j))$. $\mathcal{L}_{\text{reg}}^{\mathcal{Y}\mathcal{X}}$ and $\mathcal{L}_{\text{inlier}}^{\mathcal{Y}\mathcal{X}}$ are defined with the opposite direction $\mathcal{Y} \rightarrow \mathcal{X}$ for $\mathcal{L}_{\text{reg}}^{\mathcal{X}\mathcal{Y}}$ and $\mathcal{L}_{\text{inlier}}^{\mathcal{X}\mathcal{Y}}$, respectively.

5 Virtual Scanned MVP-RG Dataset

Existing Benchmark. First of all, we highlight that object-centric PCR is different from large-scale raw-scanned point cloud registration for the following main factors: **1)** They are mainly created for indoor or outdoor scene-level 3D point clouds, and hence are much larger-scale than object-centric PCR. **2)** They often have much more points (*e.g.* often over 30,000 points), but object-centric PPR often has around 2,000 points. **3)** They mostly have small transformations between consecutive frames. Most existing methods on object-centric PCR are evaluated on ModelNet40 (Wu et al. 2015), which consists of complete point clouds uniformly sampled from CAD model surfaces. However, their uniformly distributed points are far different from real observations that are biased by current camera pose. Specifically, view-based scans will mostly lead to partial observations and inconsistent local point densities, which makes the registration more challenging. Recently, the MVP dataset (Pan et al. 2021) consisting of multi-view virtual-scanned partial point clouds is proposed for point cloud completion, and it generates diverse partial observations for each 3D CAD model from 26 uniformly-distributed camera poses on a unit sphere. Because there are no large-scale real-scanned point clouds for object-centric registration, the proposed MVP-RG dataset makes an important step forward, which could facilitate future research on solving the sparse, noisy and challenging object-centric PPR problem.

Constructing MVP-RG. Following the MVP dataset, we establish a challenging Multi-View Partial virtual scan Registration (MVP-RG) dataset (see Fig. 1 (a)) for PPR. In the MVP-RG dataset, each partial point cloud is generated by projecting the scanned depth map to the image coordinate frame and followed by a FPS to 2,048 points. Afterwards, we select paired of partial point clouds for the same object if sufficient overlapping areas are detected. In total, our MVP-RG dataset consists of 7,600 partial point cloud pairs from 16 categories, which is split into a training set (6,400 samples) and a testing set (1,200 samples).

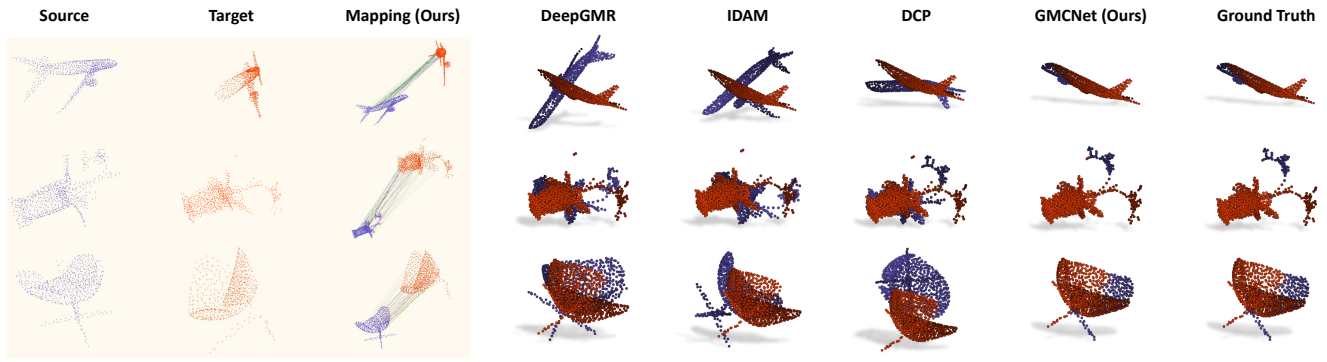


Fig. 8: Qualitative Partial-to-Partial Point Cloud Registration Results on ModelNet40 (Wu et al. 2015). 50 randomly selected correspondences by GMCNet are visualized in “Mapping”.

Properties and Advantages. Different from the MVP dataset that assumes all objects are in the same canonical pose, we randomly transform the 3D object for each observation, and hence making it a full-range PPR problem. Partial point cloud pair examples are shown in Fig. 7. Particularly, the MVP-RG settings can better adapt to 6D-pose object estimation tasks, as they often utilize a multi-camera system (e.g. BigBIRD (Singh et al. 2014)) for estimating object pose in the full SE(3) domain.

6 Experiments

Datasets. We evaluate GMCNet on partial point clouds from the ModelNet40 (Wu et al. 2015) and MVP-RG datasets. We evaluate both *restricted* rotations (i.e. $[0, 45^\circ]$) and *unrestricted* rotations (i.e. $SO(3)$) defined by an arbitrary rotation axis⁵ and a random rotation magnitude in $[0, 180^\circ]$ (Yuan et al. 2020). For all evaluated benchmarks, GMCNet achieves superior performance over previous learning-based methods.

Implementation Details. Our networks are implemented using PyTorch. We use Open3D library (Zhou et al. 2018) to implement normal estimation on-the-fly. And we set all surface normal directions orient towards the coordinate origin of the posed partial point cloud. Our models are trained using the Adam optimizer (Kingma and Ba 2014) with an initial learning rate 0.001 on an NVIDIA TITAN Xp GPU for most experiments.

Evaluation Metrics. Following (Yew and Lee 2020; Yuan et al. 2020), we use mean isotropic rotation errors \mathcal{L}_R , translation errors \mathcal{L}_t , and the root mean square error \mathcal{L}_{RMSE} that evaluates registration in the context of scene reconstruction: $\mathcal{L}_R = \arccos(\frac{1}{2}(tr(\mathbf{R}_{GT}^{-1} \cdot \mathbf{R}_{pred.}) - 1))$, $\mathcal{L}_t = \|\mathbf{t}_{GT} - \mathbf{t}_{pred.}\|_2$, and $\mathcal{L}_{RMSE} = \frac{1}{N} \sqrt{\sum_{i=1}^N \|\mathbf{T}_{GT}(x_i) - \mathbf{T}_{pred.}(x_i)\|^2}$. Note that we use all points to compute \mathcal{L}_{RMSE} .

RI Features. **1) RRI** features require at least two neighbors (Chen et al. 2019) (you can check their original paper, and in their Eq. (6), $j \neq k$), and therefore we use two neighbors to encode RRI features (feature channel size $C = 8$) in the RI feature graphs of TPT modules. **2) FPFH** features are constructed by using many neighboring points, and its feature channel size $C = 33$. We use the implementation by open3D (Zhou et al. 2018). The FPFH features are only used for the input node features, and we use PPF for TPT modules, because it is very inefficient to construct FPFH for all network layers. **3) PPF** uses the estimated surface normals on-the-fly by open3D (Zhou et al. 2018). For the RI feature graphs in TPT modules, each point pair is used to encode one PPF ($C = 4$).

6.1 Registration on ModelNet40

ModelNet40 (Wu et al. 2015) contains CAD models of 40 categories, which is split into 9,843 shapes for training and 2,468 for testing. For each 3D shape, we uniformly sample 1,024 points from its surfaces. To imitate partial scans, incomplete point clouds are generated by selecting the most nearest 768 points for a randomly placed point in the space (Wang and Solomon 2019b). Following previous works (Wang and Solomon 2019a; Yuan et al. 2020; Yew and Lee 2020), we use four different data settings: 1) “Clean”, 2) “Unseen”, 3) “Noisy” and “Noisy & Unseen”, which are reported in Table 1 and Table 2, respectively. Moreover, we evaluate both restricted rotations “[0, 45°]” and unrestricted rotations “[0, 180°]” for each data setting. To achieve fair comparisons, we use the same rotation augmentations - that is [0, 45°] for restricted rotations and [0, 180°] for the unrestricted, for all reported methods. For all the other settings, we use their official configurations on ModelNet40, which are provided by the authors. All models are trained with 200 epochs. Note that many methods may use both handcrafted RI features and spatial coordinate fea-

⁵ Opposite axis directions are equivalent to rotations in $[-180^\circ, 0]$

Table 1: Partial-to-Partial Point Cloud Registration on ModelNet40 (Clean and Unseen). † denotes ground truth correspondences or cross-contextual information are used during training.

	Clean						Unseen					
	[0, 45°]			[0, 180°]			[0, 45°]			[0, 180°]		
	\mathcal{L}_R	\mathcal{L}_t	\mathcal{L}_{RMSE}	\mathcal{L}_R	\mathcal{L}_t	\mathcal{L}_{RMSE}	\mathcal{L}_R	\mathcal{L}_t	\mathcal{L}_{RMSE}	\mathcal{L}_R	\mathcal{L}_t	\mathcal{L}_{RMSE}
PRNet [†] (Wang and Solomon 2019b)	8.00°	0.054	0.073	98.16°	0.325	0.543	3.19°	0.028	0.036	91.94°	0.297	0.545
IDAM [†] (GNN) (Li et al. 2019)	1.66°	0.009	0.013	25.36°	0.126	0.166	1.61°	0.010	0.014	20.80°	0.112	0.146
IDAM [†] (FPFH) (Li et al. 2019)	0.93°	0.005	0.007	18.06°	0.083	0.115	0.86°	0.005	0.007	16.17°	0.073	0.106
RGM [†] (Fu et al. 2021)	0.30°	0.002	0.003	24.10°	0.115	0.160	0.34°	0.004	0.004	8.78°	0.076	0.084
Predator [†] (Huang et al. 2021)	1.60°	0.012	0.015	15.33°	0.041	0.077	1.32°	0.009	0.012	11.59°	0.032	0.058
DCP (Wang and Solomon 2019a)	10.24°	0.071	0.103	70.51°	0.186	0.425	11.92°	0.076	0.119	67.39°	0.170	0.410
DeepGMR (RRI) (Yuan et al. 2020)	16.95°	0.070	0.122	45.38°	0.210	0.321	17.45°	0.074	0.130	49.23°	0.219	0.349
DeepGMR (XYZ) (Yuan et al. 2020)	6.60°	0.050	0.065	67.81°	0.244	0.416	8.05°	0.053	0.074	72.27°	0.245	0.449
RPMNet (PPF) (Yew and Lee 2020)	0.78°	0.005	0.006	15.84°	0.070	0.098	0.60°	0.004	0.005	16.91°	0.079	0.127
GMCNet (RRI)	0.013°	<0.0001	<0.0001	0.036°	0.0002	0.0002	0.017°	<0.0001	<0.0001	0.053°	0.0004	0.0005
GMCNet (FPFH)	0.012°	<0.0001	<0.0001	0.253°	0.0008	0.0016	0.014°	<0.0001	<0.0001	0.549°	0.0024	0.0033
GMCNet (PPF)	0.016°	<0.0001	<0.0001	0.284°	0.0011	0.0017	0.026°	0.0002	0.0002	0.388°	0.0024	0.0030

Table 2: Partial-to-Partial Point Cloud Registration on ModelNet40 (Noisy and Unseen). † denotes ground truth correspondences or cross-contextual information are used during training. *NC* denotes Not-Converge, and it means the network does not converge during training.

	Noisy						Noisy & Unseen					
	[0, 45°]			[0, 180°]			[0, 45°]			[0, 180°]		
	\mathcal{L}_R	\mathcal{L}_t	\mathcal{L}_{RMSE}	\mathcal{L}_R	\mathcal{L}_t	\mathcal{L}_{RMSE}	\mathcal{L}_R	\mathcal{L}_t	\mathcal{L}_{RMSE}	\mathcal{L}_R	\mathcal{L}_t	\mathcal{L}_{RMSE}
PRNet [†] (Wang and Solomon 2019b)	4.37°	0.034	0.045	95.80°	0.319	0.542	8.47°	0.061	0.081	<i>NC</i>	<i>NC</i>	<i>NC</i>
IDAM [†] (GNN) (Li et al. 2019)	4.46°	0.029	0.039	57.85°	0.253	0.374	4.25°	0.025	0.037	48.23°	0.182	0.333
IDAM [†] (FPFH) (Li et al. 2019)	9.60°	0.052	0.084	71.06°	0.217	0.430	9.50°	0.051	0.087	66.01°	0.198	0.420
RGM [†] (Fu et al. 2021)	2.21°	0.013	0.018	23.58°	0.111	0.156	2.62°	0.025	0.030	25.65°	0.117	0.179
Predator [†] (Huang et al. 2021)	3.33°	0.018	0.026	40.64°	0.110	0.207	2.91°	0.017	0.024	34.32°	0.090	0.179
DCP (Wang and Solomon 2019a)	9.33°	0.070	0.097	73.61°	0.185	0.441	10.58°	0.072	0.109	75.34°	0.192	0.467
DeepGMR (RRI) (Yuan et al. 2020)	16.96°	0.068	0.120	68.68°	0.248	0.419	17.67°	0.067	0.131	41.60°	0.153	0.308
DeepGMR (XYZ) (Yuan et al. 2020)	6.48°	0.049	0.064	70.26°	0.246	0.428	7.55°	0.052	0.071	70.26°	0.233	0.436
RPMNet (PPF) (Yew and Lee 2020)	3.52°	0.214	0.029	37.82°	0.132	0.250	3.80°	0.022	0.032	39.52°	0.129	0.271
GMCNet (RRI)	1.28°	0.009	0.011	50.62°	0.206	0.315	1.47°	0.010	0.012	51.49°	0.200	0.335
GMCNet (FPFH)	1.18°	0.008	0.010	25.95°	0.115	0.184	1.33°	0.009	0.011	33.21°	0.140	0.242
GMCNet (PPF)	0.94°	0.007	0.008	18.13°	0.093	0.132	1.12°	0.008	0.010	21.63°	0.111	0.169

tures $XYZ + \Delta XYZ$, although only different *RI* features are highlighted.

Unseen Shape Point Cloud Registration. We use point clouds from all the 40 categories of ModelNet40 for training and testing. Note that all the objects used for testing have not been seen during training, and therefore in this setting we evaluate the PPR for unseen 3D shapes. As reported in Table 1, GMCNet using different *RI* features, *RRI*, *FPFH* and *PPF*, achieves nearly perfect registration results, even for full-range (*i.e.*, [0, 180°]) PPR, which challenges previous SoTA methods. Qualitative results are shown in Fig. 8, and GMCNet could estimate correct pose-invariant correspondences for registration.

Unseen Category Point Cloud Registration. In this setting, we train our network by using 3D point clouds from the

first 20 categories, and use the other 20 category point clouds for evaluation. Because GMCNet learns to encode local transformation-robust geometrical features that do not rely on the global shape category information heavily, it shows great generalizability for registering point clouds from unseen categories. Similar with the ‘‘Clean’’ setting, GMCNet significantly outperforms existing SoTA methods in Table 1, especially for ‘‘Unseen’’ full-range PPR.

Noisy Point Cloud Registration. Following previous methods, we add Gaussian noise that are randomly sampled from $\mathcal{N}(0, 0.01)$ and clipped to $[-0.05, 0.05]$ to partial point clouds for evaluating PPR under random noise. By adding random noise, raw handcrafted *RI* features become no longer transformation-invariant, which mostly influences the global registration performance. In our experiments re-

Table 3: Input Feature Analysis. Handcrafted rotation-invariant features (*RRI*, *FPFH*, and *PPF*) and “XYZ+ Δ XYZ” features. ‡ denotes the issue “svd did not converge” occurred.

Input Features	Rotation Ranges	Clean			Unseen			Noise		
		\mathcal{L}_R	\mathcal{L}_t	\mathcal{L}_{RMSE}	\mathcal{L}_R	\mathcal{L}_t	\mathcal{L}_{RMSE}	\mathcal{L}_R	\mathcal{L}_t	\mathcal{L}_{RMSE}
<i>RRI</i> Only	[0, 45°]	0.015°	<0.0001	<0.0001	0.023°	0.0002	0.0002	10.50°	0.050	0.075
	[0, 180°]	0.021°	0.0001	0.0001	0.043°	0.0003	0.0003	49.12°	0.201	0.306
<i>RRI</i> + XYZ + Δ XYZ	[0, 45°]	0.013°	< 0.0001	< 0.0001	0.017°	< 0.0001	< 0.0001	1.28°	0.009	0.011
	[0, 180°]	0.036°	0.0002	0.0002	0.053°	0.0004	0.0005	50.62°	0.206	0.315
<i>FPFH</i> Only	[0, 45°]	0.206°	0.0024	0.0025	0.387°	0.0038	0.0041	7.97°	0.045	0.065
	[0, 180°]	2.43°‡	0.0203‡	0.0223‡	2.33°‡	0.0200‡	0.0226‡	29.93°	0.130	0.210
<i>FPFH</i> + XYZ + Δ XYZ	[0, 45°]	0.012°	< 0.0001	< 0.0001	0.014°	< 0.0001	< 0.0001	1.18°	0.008	0.010
	[0, 180°]	0.253°	0.0008	0.0016	0.549°	0.0024	0.0033	25.95°	0.115	0.184
<i>PPF</i> Only	[0, 45°]	0.017°	0.0002	0.0002	0.039°	0.0005	0.0005	4.41°	0.030	0.038
	[0, 180°]	0.258°	0.0020	0.0023	0.238°	0.0017	0.0018	23.13°	0.116	0.168
<i>PPF</i> + XYZ + Δ XYZ	[0, 45°]	0.016°	< 0.0001	< 0.0001	0.026°	0.0002	0.0002	0.94°	0.007	0.008
	[0, 180°]	0.284°	0.0011	0.0017	0.388°	0.0024	0.0030	18.13°	0.093	0.132

ported in Table 2, GMCNet could resolve local PPR with small registration error, and also achieves better global registration with the help of *PPF* than previous SoTA methods. Because we are focused on encoding geometrical features from local structures of the 3D shapes, those symmetric shapes and repetitive structures (*e.g.* vases and tables) of 3D shapes from ModelNet40 dataset give rise to challenges, such as plausible feature correspondences or local optima, in resolving noisy full-range PPR.

Unseen Category and Noisy Point Cloud Registration.

The “Unseen & Noisy” setting is a combination of “Unseen” and “Noisy”: Firstly, we train networks with 3D objects from the first 20 categories, and then test on the rest 20 categories; additionally, random noise sampled from Gaussian distribution $\mathcal{N}(0, 0.01)$ that is clipped to $[-0.05, 0.05]$, is added to the partial point clouds. Similar with the “Noisy” setting, the proposed GMCNet could resolve local registration very well, but also struggles with global registration. Even though, GMCNet achieves better registration than previous SoTA methods for most evaluated metrics.

Different Rotation-Invariant (RI) Features. In Table 1 and Table 2, we evaluated *RRI*, *FPFH* and *PPF* in GMCNet. Although *RRI* features are no longer consistent for clean partial point clouds under different SE(3) transformations due to center shifting (as discussed in Sec. 3), GMCNet estimate faithful correspondences between different partial point clouds for PPR. We think the reason is that the inconsistency caused by translations influences the encoded *RRI* features for all points, which is compensated during the feature matching optimization if perfect correspondences exist. Together with random noise, local registration with *RRI* features can be resolved mainly due to using spatial coordinates graphs. However, it is too challenging to use *RRI* for global

Table 4: Ablation studies for full-range Partial-to-Partial Point Cloud Registration on ModelNet40 (“Clean”).

K-NN	TPT	HGM	$\mathcal{L}_R \downarrow$	$\mathcal{L}_t \downarrow$	$\mathcal{L}_{RMSE} \downarrow$
			36.93°	0.197	0.286
✓			9.01°	0.048	0.065
✓	✓		5.85°	0.036	0.065
✓	✓	✓	0.016°	<0.0001	<0.0001

PPR with noisy data, while those local *RI* features, *FPFH* and *PPF*, can lead to better registration results.

Effectiveness of Different Input Features. We evaluate the effectiveness of different input feature elements, including *RRI*, *FPFH*, *PPF*, XYZ and Δ XYZ, in Table 3. Obviously, all handcrafted *RI* features can resolve full-range registration with clean data (“Clean” and “Unseen”), and using *RRI* features achieves slightly better performance than using *PPF* or *FPFH*. We think it is because the center shifting problem of *RRI* features can be compensated during optimization, while surface normal direction ambiguities cannot. However, they perform differently with noisy point clouds (“Noisy”). With small relative transformations (*i.e.* [0, 45°]), using spatial coordinate features XYZ + Δ XYZ significantly improves PPR performance for all handcrafted *RI* features. For large relative transformations (*i.e.* [0, 180°]), the PPR problem is too challenging to be fully resolved. The global *RI* feature, *RRI*, performs the worst on noisy point clouds than the other local *RI* features, *FPFH* and *PPF*. Comparing to *FPFH*, *PPF* is preferred due to 1) it achieves better performance; and 2) it is more convenient to construct in terms of time efficiency. We think the main challenges for global PPR with noisy data are that

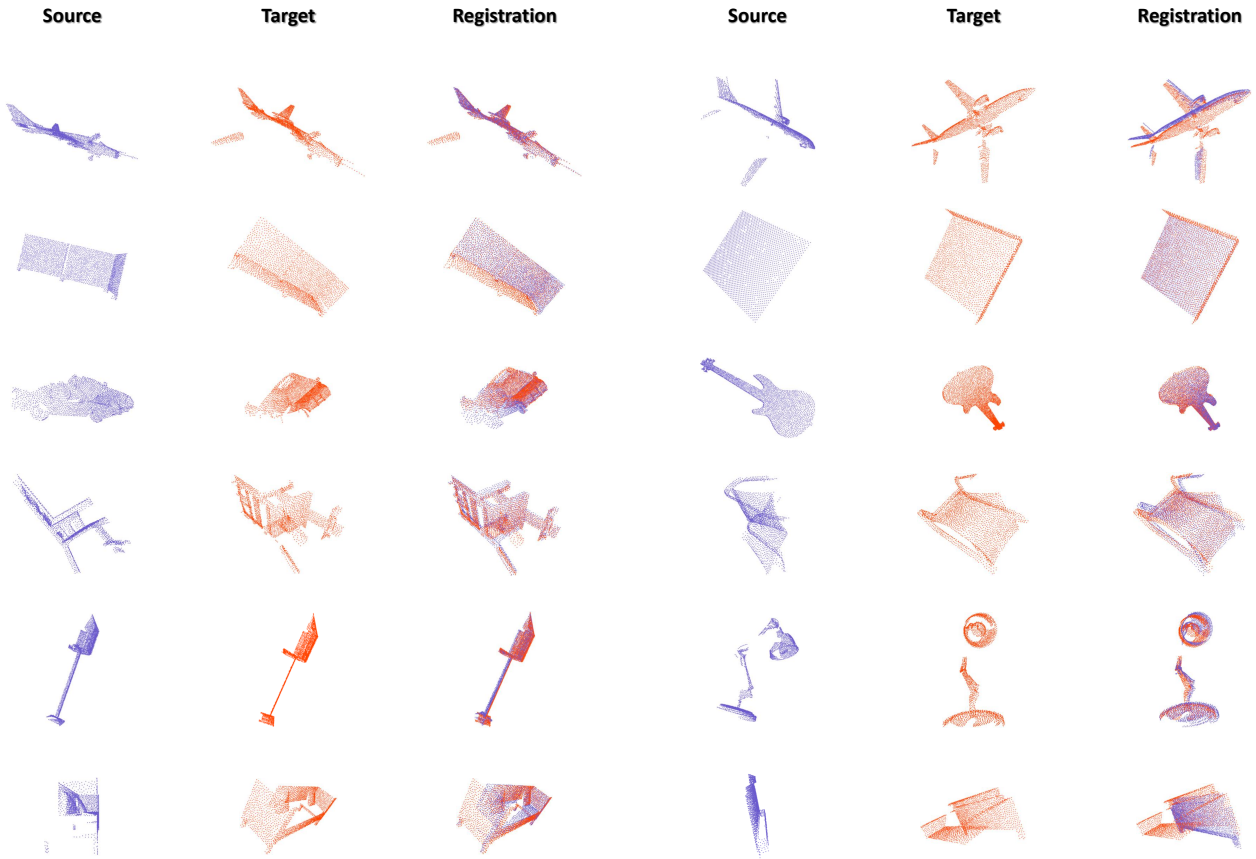


Fig. 9: Partial-to-Partial Point Cloud Registration Results by GMCNet on MVP-RG Dataset.

many objects in ModelNet40 and MVP-RG 1) are rotational symmetric; or 2) have repetitive similar structures. Hence, if there are few or no perfect correspondences caused by noise, PPR can often converge to other alignment results rather than the ground truth. For image feature matching, recent methods, such as R2D2 (Revaud et al. 2019) and SuperGlue (Sarlin et al. 2020), are proposed, which can be a promising future research direction for 3D feature matching.

Ablation Study. We report ablation studies on the main components of GMCNet, including using K-NN graphs, TPT modules and HGM architecture, in Table 4. The baseline model directly uses *PPF* features for registration. With the help of K-NN graphs, the encoded features become more discriminative, and hence leading to much better registration. Using TPT modules further improves registration performance. Moreover, HGM introduces large-scale graph-based relations based on TPT and the hierarchical architecture, which perfectly resolves most PPR with clean data. In case that readers are curious about the effectiveness of using *RI* features, we further report two ablation settings, **1) *RI* features + RANSAC:** we try to match *PPF* by using RANSAC with 4 million iterations by tuning different inlier ratio settings. The better results of RANSAC(4M) are

14.69° (\mathcal{L}_R), 0.149 (\mathcal{L}_t), and 0.159 (\mathcal{L}_{RMSE}) on the ModelNet40 with the “Clean” settings. Because RANSAC cannot adapt to different inlier ratios, registration by RANSAC(4M) is much worse than GMCNet. **2) No *RI* features:** As they are the key components of our methods, without using *RI* features, OM could not converge under large transformations. Note that GMCNet does not explicitly supervise the corresponding feature points to have similar feature descriptors during training, but *RI* features, especially local *RI* features, could provide the geometrical clues.

6.2 Registration on MVP-RG

We further evaluate GMCNet on the MVP-RG dataset consisting of view-based partial point clouds (see Fig. 7). Note that the partial point cloud pairs can have no perfect correspondences, since different partial point clouds are generated by different scans from various camera views. Hence, registering partial point clouds from MVP-RG dataset is a noisy full-range PPR problem. To achieve fair comparisons, we use the same rotation augmentations for all methods, and use their best settings that previously are used for PPR with noisy data from ModelNet40. All models are trained

Table 5: Partial-to-Partial Point Cloud Registration on MVP-RG.

	\mathcal{L}_R	\mathcal{L}_t	\mathcal{L}_{RMSE}
IDAM [†] (GNN) (Li et al. 2019)	24.35°	0.280	0.344
IDAM [†] (FPFH) (Li et al. 2019)	35.78°	0.391	0.476
RGM [†] (Fu et al. 2021)	41.27°	0.425	0.583
DCP (Wang and Solomon 2019a)	30.37°	0.273	0.634
DeepGMR (RRJ) (Yuan et al. 2020)	49.72°	0.385	0.696
DeepGMR (XYZ) (Yuan et al. 2020)	43.74°	0.353	0.608
RPMNet (PPF) (Yew and Lee 2020)	22.20°	0.174	0.327
GMCNet (PPF)	16.57°	0.174	0.246

with 200 epochs. Similarly, it is very challenging to register noisy partial point clouds for MVP-RG. As reported in Table 5, GMCNet still outperforms previous SoTA methods on MVP-RG. Qualitative registration results are shown in Fig. 9.

7 Conclusion and Discussion

In this work, we propose a comprehensive paradigm GMCNet, which utilizes a synergy of hierarchical graph networks and graphical modeling for object-centric PPR. In particular, we provide an in-depth analysis on the rotation-invariance and noise-resilience for handcrafted features, based on which we propose a novel TPT model to adaptively aggregate neighboring features. Furthermore, we establish a challenging virtual-scanned partial point cloud dataset MVP-RG. Extensive experiments show that GMCNet outperforms previous SoTA methods.

We want to highlight that in line with previous settings that evaluating object-centric PCR problem under local transformations ($[0, 45^\circ]$), our GMCNet achieves much better registration results and almost perfectly resolve all the challenging PPR problems. Furthermore, we evaluate on global registration problem ($[0, 180^\circ]$), and the proposed GMCNet addresses most PPR problems excepting for registering those noisy partial point clouds (e.g. ModelNet40(Noisy) and MVP-RG). Even though, GMCNet still outperforms previous methods. For future research, we encourage that researchers can learn to detect discriminative feature points by considering cross-contextual geometric information between the paired point clouds, analogy to image feature matching counterparts (Revaud et al. 2019; Sarlin et al. 2020). We hope our study on learning transformation-robust point descriptors from handcrafted *RI* features and the established MVP-RG dataset can inspire future research for 3D point cloud registration.

Acknowledgments

This work is supported by NTU NAP, MOE AcRF Tier 2 (T2EP20221-0033), and under the RIE2020 Industry Alignment Fund – Industry Collaboration Projects (IAF-ICP) Funding Initiative, as well as cash and in-kind contribution from the industry partner(s).

References

- Aoki Y, Goforth H, Srivatsan RA, Lucey S (2019) Pointnetlk: Robust & efficient point cloud registration using pointnet. In: Proceedings of the IEEE Conference on Computer Vision and Pattern Recognition, pp 7163–7172 3
- Bai X, Luo Z, Zhou L, Fu H, Quan L, Tai CL (2020) D3feat: Joint learning of dense detection and description of 3d local features. In: Proceedings of the IEEE/CVF Conference on Computer Vision and Pattern Recognition, pp 6359–6367 3
- Bauer D, Patten T, Vincze M (2021) Reagent: Point cloud registration using imitation and reinforcement learning. In: Proceedings of the IEEE/CVF Conference on Computer Vision and Pattern Recognition, pp 14586–14594 3
- Besl PJ, McKay ND (1992) Method for registration of 3-d shapes. In: Sensor fusion IV: control paradigms and data structures, International Society for Optics and Photonics, vol 1611, pp 586–606 3
- Bouaziz S, Tagliasacchi A, Pauly M (2013) Sparse iterative closest point. In: Computer graphics forum, Wiley Online Library, vol 32, pp 113–123 3
- Chen C, Li G, Xu R, Chen T, Wang M, Lin L (2019) Cluster-net: Deep hierarchical cluster network with rigorously rotation-invariant representation for point cloud analysis. In: Proceedings of the IEEE/CVF Conference on Computer Vision and Pattern Recognition, pp 4994–5002 2, 3, 4, 5, 9
- Chen H, Bhanu B (2007) 3d free-form object recognition in range images using local surface patches. Pattern Recognition Letters 28(10):1252–1262 3
- Choy C, Park J, Koltun V (2019) Fully convolutional geometric features. In: Proceedings of the IEEE/CVF International Conference on Computer Vision, pp 8958–8966 3
- Deng H, Birdal T, Ilic S (2018a) Ppf-foldnet: Unsupervised learning of rotation invariant 3d local descriptors. In: Proceedings of the European Conference on Computer Vision (ECCV), pp 602–618 3
- Deng H, Birdal T, Ilic S (2018b) Ppfnet: Global context aware local features for robust 3d point matching. In: Proceedings of the IEEE conference on computer vision and pattern recognition, pp 195–205 3, 5, 7
- Ding L, Feng C (2019) Deepmapping: Unsupervised map estimation from multiple point clouds. In: Proceedings of the IEEE Conference on Computer Vision and Pattern Recognition, pp 8650–8659 1
- Droeschel D, Behnke S (2018) Efficient continuous-time slam for 3d lidar-based online mapping. In: 2018 IEEE International Conference on Robotics and Automation (ICRA), IEEE, pp 1–9 1
- Drost B, Ulrich M, Navab N, Ilic S (2010) Model globally, match locally: Efficient and robust 3d object recognition. In: 2010 IEEE computer society conference on computer vision and pattern recognition, Ieee, pp 998–1005 2, 3, 4
- Frome A, Huber D, Kolluri R, Bülow T, Malik J (2004) Recognizing objects in range data using regional point descriptors. In: European conference on computer vision, Springer, pp 224–237 3
- Fu K, Liu S, Luo X, Wang M (2021) Robust point cloud registration framework based on deep graph matching. In: Proceedings of the

- IEEE/CVF Conference on Computer Vision and Pattern Recognition, pp 8893–8902 [1](#), [10](#), [13](#)
- Fuchs F, Worrall D, Fischer V, Welling M (2020) Se (3)-transformers: 3d roto-translation equivariant attention networks. *Advances in Neural Information Processing Systems* [33](#) [2](#)
- Gojcic Z, Zhou C, Wegner JD, Wieser A (2019) The perfect match: 3d point cloud matching with smoothed densities. In: *Proceedings of the IEEE/CVF Conference on Computer Vision and Pattern Recognition*, pp 5545–5554 [3](#)
- Guo MH, Cai JX, Liu ZN, Mu TJ, Martin RR, Hu SM (2021) Pct: Point cloud transformer. *Computational Visual Media* [7](#)(2):187–199 [6](#)
- Huang S, Gojcic Z, Usvatsov M, Wieser A, Schindler K (2021) Predator: Registration of 3d point clouds with low overlap. In: *Proceedings of the IEEE/CVF Conference on Computer Vision and Pattern Recognition*, pp 4267–4276 [10](#)
- Jiang H, Shen Y, Xie J, Li J, Qian J, Yang J (2021) Sampling network guided cross-entropy method for unsupervised point cloud registration. In: *Proceedings of the IEEE/CVF International Conference on Computer Vision*, pp 6128–6137 [3](#)
- Johnson AE, Hebert M (1999) Using spin images for efficient object recognition in cluttered 3d scenes. *IEEE Transactions on pattern analysis and machine intelligence* [21](#)(5):433–449 [3](#)
- Kingma DP, Ba J (2014) Adam: A method for stochastic optimization. *arXiv preprint arXiv:1412.6980* [9](#)
- Koller D, Friedman N (2009) *Probabilistic graphical models: principles and techniques*. MIT press [7](#)
- Li J, Zhang C, Xu Z, Zhou H, Zhang C (2019) Iterative distance-aware similarity matrix convolution with mutual-supervised point elimination for efficient point cloud registration. *arXiv preprint arXiv:191010328* [1](#), [2](#), [3](#), [4](#), [5](#), [10](#), [13](#)
- Li X, Kaesemodel Pontes J, Lucey S (2020) Deterministic pointnetlk for generalized registration. *arXiv e-prints* pp arXiv–2008 [3](#)
- Li X, Li R, Chen G, Fu CW, Cohen-Or D, Heng PA (2021) A rotation-invariant framework for deep point cloud analysis. *IEEE Transactions on Visualization and Computer Graphics* [2](#), [5](#)
- Lu W, Zhou Y, Wan G, Hou S, Song S (2019) L3-net: Towards learning based lidar localization for autonomous driving. In: *Proceedings of the IEEE Conference on Computer Vision and Pattern Recognition*, pp 6389–6398 [1](#)
- Maron H, Dym N, Kezurer I, Kovalsky S, Lipman Y (2016) Point registration via efficient convex relaxation. *ACM Transactions on Graphics (TOG)* [35](#)(4):1–12 [3](#)
- Pan L, Chen X, Cai Z, Zhang J, Zhao H, Yi S, Liu Z (2021) Variational relational point completion network. In: *Proceedings of the IEEE/CVF Conference on Computer Vision and Pattern Recognition*, pp 8524–8533 [3](#), [8](#)
- Pomerleau F, Colas F, Siegwart R, et al. (2015) A review of point cloud registration algorithms for mobile robotics. *Foundations and Trends® in Robotics* [4](#)(1):1–104 [3](#)
- Qi CR, Su H, Mo K, Guibas LJ (2017) Pointnet: Deep learning on point sets for 3d classification and segmentation. *Proc Computer Vision and Pattern Recognition (CVPR)*, IEEE [1](#)(2):4 [3](#)
- Revaud J, Weinzaepfel P, De Souza C, Pion N, Csurka G, Cabon Y, Humenberger M (2019) R2d2: repeatable and reliable detector and descriptor. *arXiv preprint arXiv:190606195* [12](#), [13](#)
- Rusinkiewicz S, Levoy M (2001) Efficient variants of the icp algorithm. In: *Proceedings Third International Conference on 3-D Digital Imaging and Modeling*, IEEE, pp 145–152 [3](#)
- Rusu RB, Blodow N, Marton ZC, Beetz M (2008) Aligning point cloud views using persistent feature histograms. In: *2008 IEEE/RSJ international conference on intelligent robots and systems*, IEEE, pp 3384–3391 [3](#)
- Rusu RB, Blodow N, Beetz M (2009) Fast point feature histograms (fpfh) for 3d registration. In: *2009 IEEE international conference on robotics and automation*, IEEE, pp 3212–3217 [3](#), [4](#)
- Salti S, Tombari F, Di Stefano L (2014) Shot: Unique signatures of histograms for surface and texture description. *Computer Vision and Image Understanding* [125](#):251–264 [3](#)
- Santa Cruz R, Fernando B, Cherian A, Gould S (2017) Deeppermnet: Visual permutation learning. In: *Proceedings of the IEEE Conference on Computer Vision and Pattern Recognition*, pp 3949–3957 [8](#)
- Sarlin PE, DeTone D, Malisiewicz T, Rabinovich A (2020) Superglue: Learning feature matching with graph neural networks. In: *Proceedings of the IEEE/CVF conference on computer vision and pattern recognition*, pp 4938–4947 [8](#), [12](#), [13](#)
- Sarode V, Li X, Goforth H, Aoki Y, Dhagat A, Srivatsan RA, Lucey S, Choset H (2019a) One framework to register them all: Pointnet encoding for point cloud alignment. *arXiv preprint arXiv:191205766* [3](#)
- Sarode V, Li X, Goforth H, Aoki Y, Srivatsan RA, Lucey S, Choset H (2019b) Pcnnet: Point cloud registration network using pointnet encoding. *arXiv preprint arXiv:190807906* [3](#)
- Satorras VG, Hoogeboom E, Fuchs FB, Posner I, Welling M (2021) E (n) equivariant normalizing flows for molecule generation in 3d. *arXiv preprint arXiv:210509016* [2](#)
- Segal A, Haehnel D, Thrun S (2009) Generalized-icp. In: *Robotics: science and systems*, Seattle, WA, vol 2, p 435 [3](#)
- Singh A, Sha J, Narayan KS, Achim T, Abbeel P (2014) Bigbird: A large-scale 3d database of object instances. In: *2014 IEEE international conference on robotics and automation (ICRA)*, IEEE, pp 509–516 [9](#)
- Sun W, Tagliasacchi A, Deng B, Sabour S, Yazdani S, Hinton G, Yi KM (2020) Canonical capsules: Unsupervised capsules in canonical pose. *arXiv preprint arXiv:201204718* [3](#)
- Tian M, Pan L, Ang MH, Lee GH (2020) Robust 6d object pose estimation by learning rgb-d features. In: *2020 IEEE International Conference on Robotics and Automation (ICRA)*, IEEE, pp 6218–6224 [1](#)
- Tombari F, Salti S, Di Stefano L (2010) Unique shape context for 3d data description. In: *Proceedings of the ACM workshop on 3D object retrieval*, pp 57–62 [3](#)
- Vaswani A, Shazeer N, Parmar N, Uszkoreit J, Jones L, Gomez AN, Kaiser Ł, Polosukhin I (2017) Attention is all you need. In: *Advances in neural information processing systems*, pp 5998–6008 [6](#)
- Wan G, Yang X, Cai R, Li H, Zhou Y, Wang H, Song S (2018) Robust and precise vehicle localization based on multi-sensor fusion in diverse city scenes. In: *2018 IEEE International Conference on Robotics and Automation (ICRA)*, IEEE, pp 4670–4677 [1](#)
- Wang Y, Solomon JM (2019a) Deep closest point: Learning representations for point cloud registration. In: *Proceedings of the IEEE International Conference on Computer Vision*, pp 3523–3532 [1](#), [2](#), [3](#), [4](#), [9](#), [10](#), [13](#)
- Wang Y, Solomon JM (2019b) Pcnnet: Self-supervised learning for partial-to-partial registration. In: *Advances in Neural Information Processing Systems*, pp 8812–8824 [1](#), [3](#), [4](#), [9](#), [10](#)
- Wang Y, Sun Y, Liu Z, Sarma SE, Bronstein MM, Solomon JM (2019) Dynamic graph cnn for learning on point clouds. *ACM Transactions on Graphics (TOG)* [38](#)(5):1–12 [3](#)
- Wong JM, Kee V, Le T, Wagner S, Mariottini GL, Schneider A, Hamilton L, Chipalkatty R, Hebert M, Johnson DM, et al. (2017) Segicp: Integrated deep semantic segmentation and pose estimation. In: *2017 IEEE/RSJ International Conference on Intelligent Robots and Systems (IROS)*, IEEE, pp 5784–5789 [1](#)
- Wu Z, Song S, Khosla A, Yu F, Zhang L, Tang X, Xiao J (2015) 3d shapenets: A deep representation for volumetric shapes. In: *Proceedings of the IEEE conference on computer vision and pattern recognition*, pp 1912–1920 [1](#), [2](#), [3](#), [8](#), [9](#)
- Xu H, Liu S, Wang G, Liu G, Zeng B (2021) Omnet: Learning overlapping mask for partial-to-partial point cloud registration. *arXiv*

- preprint arXiv:210300937 3
- Yang H, Carlone L (2019) A polynomial-time solution for robust registration with extreme outlier rates. arXiv preprint arXiv:190308588 3
- Yang J, Li H, Jia Y (2013) Go-icp: Solving 3d registration efficiently and globally optimally. In: Proceedings of the IEEE International Conference on Computer Vision, pp 1457–1464 3
- Yang S, Zhu X, Nian X, Feng L, Qu X, Mal T (2018) A robust pose graph approach for city scale lidar mapping. In: 2018 IEEE/RSJ International Conference on Intelligent Robots and Systems (IROS), IEEE, pp 1175–1182 1
- Yew ZJ, Lee GH (2020) Rpm-net: Robust point matching using learned features. In: Proceedings of the IEEE/CVF conference on computer vision and pattern recognition, pp 11824–11833 1, 2, 3, 4, 5, 7, 8, 9, 10, 13
- Yuan W, Eckart B, Kim K, Jampani V, Fox D, Kautz J (2020) Deepgmr: Learning latent gaussian mixture models for registration. In: European Conference on Computer Vision, Springer, pp 733–750 1, 2, 3, 5, 9, 10, 13
- Zhang Z, Hua BS, Rosen DW, Yeung SK (2019) Rotation invariant convolutions for 3d point clouds deep learning. In: International Conference on 3D Vision (3DV) 4, 5
- Zhang Z, Hua BS, Yeung SK (2022) Riconv++: Effective rotation invariant convolutions for 3d point clouds deep learning. International Journal of Computer Vision pp 1–16 5
- Zhao H, Jia J, Koltun V (2020) Exploring self-attention for image recognition. In: Proceedings of the IEEE/CVF Conference on Computer Vision and Pattern Recognition, pp 10076–10085 6
- Zhao H, Jiang L, Jia J, Torr PH, Koltun V (2021) Point transformer. In: Proceedings of the IEEE/CVF International Conference on Computer Vision, pp 16259–16268 6
- Zhao Y, Birdal T, Deng H, Tombari F (2019) 3d point capsule networks. In: Proceedings of the IEEE/CVF Conference on Computer Vision and Pattern Recognition, pp 1009–1018 3
- Zhou QY, Park J, Koltun V (2016) Fast global registration. In: European Conference on Computer Vision, Springer, pp 766–782 3
- Zhou QY, Park J, Koltun V (2018) Open3d: A modern library for 3d data processing. arXiv preprint arXiv:180109847 9